Final Draft
of the original manuscript:

Scheider, I.:
Derivation of separation laws for cohesive models in the course of ductile fracture
In: Engineering Fracture Mechanics (2008) Elsevier

DOI: 10.1016/j.engfracmech.2008.12.006

Derivation of separation laws for cohesive models in the course of ductile fracture

Ingo Scheider, GKSS Research Centre Geesthacht GmbH, Member of the Helmholtz Association, Institute for Materials Research

Abstract

The paper addresses the determination of the traction-separation law of the cohesive model on a micromechanical basis. For this task, a specific failure mechanism, i.e. ductile damage consisting of void nucleation, growth and coalescence, is investigated. An approach already described in the literature is to transfer the deformation behaviour of the most simple representative volume element, i.e. a single voided unit cell, to the cohesive interface. After reviewing the existing approach, its main drawback, namely that the unit cell contains both, deformation and damage of a material point whereas the cohesive model should contain the material separation only, is addressed. A new approach is presented, in which the behaviour of a unit cell is divided in its elasto-plastic deformation and damage, and only the damage is applied as traction-separation law for the cohesive model. Instead of modelling the voided unit cell, a single element with Gurson type plastic potential for the damage has been employed as a reference for the behaviour at the micro scale. A study with fracture specimens, C(T) and M(T), made of an engineering Aluminium alloy shows that the new approach exhibits a better transferability than the existing one.

Keywords:

ductile fracture cohesive modelling, GTN model, traction-separation law, unit cells

Nomenclature

B_n	nominal thickness of the fracture specimen
D_{cell}	element height of the GTN unit cell
T_0	cohesive strength
W	width of the fracture specimen (half width for M(T) specimen)
a_0	initial crack length
f	void volume fraction
f^*	damage variable of the GTN model
f_0, f_c, f_n	GTN model parameters
h	triaxiality (= σ_h / σ_{eq})
s_n	GTN model parameter
Γ_0	specific cohesive energy
Δa	crack extension
β	biaxiality ratio
δ_0	critical separation
δ_1, δ_2	shape parameters of the traction-separation law
γ	specific energy dissipated by GTN unit cell
$\bar{\varepsilon}_M^{pl}$	equivalent plastic strain of the matrix material (GTN model)
σ_{eq}	von Mises equivalent stress
σ_{appl}	applied stress for GTN unit cell simulation
σ_Y	yield strength
σ_h	hydrostatic stress (= σ_{ii}/ 3)
κ	GTN model parameter

Introduction

The main failure mechanism in ductile metals consists of the nucleation of voids and their growth and coalescence. One numerical model for the description of this damage process is the well-known Gurson model [1], which has been extended by several authors to better reproduce experimental results, see e.g. [2, 3]. The advantage of this type of models is that it has a micro-mechanical basis and can be used to predict damage and failure of the material even in initially undamaged structures. The main drawback is that they only cover this single failure mechanism and cannot be used anymore if another mechanism is activated, e.g. cleavage.

Another model to describe material failure, but on a more phenomenological basis (i.e. without considering the material's microstructure), is the cohesive model, which is based on an idea proposed by Dugdale [4] and Barenblatt [5] in the early 60's and has also been applied to ductile damage during the last 20 years starting with an investigation by Needleman [6] and followed by innumerable research groups. For details on the developments, implementations and applications, see e.g. [7].

Within the framework of cohesive modelling and finite elements, the zone in which damage occurs is reduced to a layer with zero thickness. The cohesive elements along this layer model the material separation and are placed along the supposed crack path; the surrounding continuum elements are damage-free.

The constitutive behaviour according to which the cohesive elements open and eventually fail, is described by the so-called traction-separation law, which relates the traction vector, $\mathbf{T}$, to the displacement jump, $[\mathbf{u}]$, across the interface, usually called separation, $\boldsymbol{\delta}$. The coordinate system, in which these vectors are given, is usually such that the first component describes separation normal to the interface and the other two describe the tangential separation. For mode I fracture, which is considered solely throughout this paper, the relation reduces to a scalar equation, $T(\delta)$.

The shape of this traction-separation law has been chosen by many different functions from the various research groups. Common to all shapes is that they contain two model parameters, namely the maximum traction sustainable by the element, T_0, and a critical separation, δ_0, at which the element finally fails. The energy dissipated by the element until total failure, Γ_0, is derived as the integral $\Gamma_0 = \int_0^{\delta_0} T(\delta)\,\mathrm{d}\delta$. Evidently, Γ_0 depends on the shape of $T(\delta)$.

One important question in this regard, which has been raised by many different research groups, is whether the shape of the traction-separation law has an influence on the results of the simulation, and, if yes, which shape is the correct one for a specific material. The first part of the question has been studied e.g. in [8-12]. Also, the identification of the correct shape of the traction-separation law for specific materials was investigated by different research groups. For example, if the material under consideration is purely elastic, a simple tensile test might be sufficient to determine the whole function $T(\delta)$, see [13], since every deformation that deviates from the linear elastic behaviour can be taken as material separation. Another method for the identification of T(d) based on *J*-integral and crack opening profile measurements was proposed in [14] for concrete and later used in [15] for adhesive debonding and delamination.

The above cited literature deals only with material modelling at the structural scale, i.e. based on a continuum mechanics approach. However, the cohesive model can also be used at a smaller scale, for example for particle or fibre debonding in composite materials [16, 17]. The identification of the parameters on that scale is much more difficult than for the macro scale, the determination of the shape is hardly possible at all. However, micro testing may help to get at least an estimate of the interface properties, e.g. by fibre pushout tests [18].

Beside using the cohesive model as a phenomenological crack extension model (either at the macro or at the micro scale), it is also possible to bridge the micro- and the macro scale with the cohesive model, such that the traction-separation law for the structural scale is a result of the damage process at the micro-scale. Such an approach will be presented in the following for the mechanism of ductile damage.

In order to determine this traction-separation law on a micromechanical basis, the deformation behaviour of a representative volume element, i.e. a single voided unit cell, including its material softening behaviour has been investigated in literature, see e.g. [19], where the damage behaviour of such a cell is described as cohesion-decohesion curve. The first who used this approach for the derivation of a traction-separation law in the course of cohesive modelling, were Siegmund and Brocks [20, 21], who used a Gurson type model for the unit cell. The approach was extended to impact problems by Anvari and co-workers [22]. In these studies, the results from the unit cell deformation are directly used as traction-separation law.

Another issue that becomes obvious by the microstructural investigation is that the traction-separation law depends on the stress state, which can be characterised by the triaxiality, $h = \sigma_h / \sigma_{eq}$. Evidence for constraint dependence of the cohesive parameters is also given by comparison with experiments, see e.g. [23, 24]. This dependence can easily be quantified at the microscale by loading the representative volume element under different constraint conditions, as shown in [22, 25].

The main drawback of the approach described in [20-22] is addressed, namely that the representative volume element actually contains both, deformation and damage of a material point whereas the cohesive model should contain the material separation only. This could be the reason, why results of the triaxiality dependent cohesive model reported in [25] show a worse transferability between C(T) and M(T) specimens than the cohesive model with constant parameters. A new approach is presented here, in which the behaviour of a unit cell is divided in its deformation and damage contributions, and only the damage is applied as a traction-separation law for the cohesive model. A study on the same material that was already investigated in [21, 25], a ferritic steel (German designation StE 460), shows that the results are closer to a reference simulation provided by the Gurson model than those of the existing approach.

Numerical models

Two models are used in this study, the first is the micro-mechanical damage model developed originally by Gurson and extended by Tvergaard and Needleman, the second is the cohesive model with constraint dependent parameters.

Micromechanical model for ductile damage

The failure mechanism of ductile metals is characterised by void nucleation, growth and coalescence. A simple method to model this damage process is the plastic potential derived by

Gurson 30 years ago, which has been extended by Tvergaard and Needleman to incorporate the effect of accelerated damage due to coalescence of voids. The potential is given by the well-known equation

$$\Phi = \frac{\sigma_{eq}^2}{R^2\left(\bar{\varepsilon}_M^{pl}\right)} + 2q_1 f^* \cosh\left(\frac{3\sigma_h}{2R\left(\bar{\varepsilon}_M^{pl}\right)} q_2\right) - 1 - \left(q_1 f^*\right)^2 = 0\,, \tag{1}$$

where R is the flow strength of the material surrounding the void, q_1, q_2 and q_3 are model parameters and f^* is a damage variable, which is a function of the void volume fraction, f:

$$f^* = \begin{cases} f & f \le f_c \\ f_c + \kappa\left(f - f_c\right) & f > f_c \end{cases}. \tag{2}$$

The two parameters κ and f_c are additional model parameters. The evolution of the void volume fraction consists of void growth and void nucleation, both driven by plastic straining:

$$\dot{f} = (1-f)\,\dot{\varepsilon}_{ij}^{pl}\delta_{ij} + A\dot{\bar{\varepsilon}}_M^{pl}\,, \quad A = \frac{f_n}{s_n\sqrt{2\pi}} \exp\left[-\frac{1}{2}\left(\frac{\bar{\varepsilon}_M^{pl} - \varepsilon_n}{s_n}\right)^2\right] \tag{3}$$

Together with an initial void volume fraction in the virgin material, f_0, and the three parameters for void nucleation, s_n, ε_n, f_n, the model contains 9 parameters. The equations have been implemented in the finite element system ABAQUS by Siegmund and Brocks [20] as a user defined material (UMAT).

Cohesive model

The constitutive behaviour of the cohesive model utilised here is a threefold function $T(\delta)$ for normal separation:

$$T(\delta) = T_0\, f(\delta) = T_0 \begin{cases} 2\left(\dfrac{\delta}{\delta_1}\right) - \left(\dfrac{\delta}{\delta_1}\right)^2 & \delta < \delta_1 \\ 1 & \delta_1 < \delta < \delta_2 \\ 2\left(\dfrac{\delta - \delta_2}{\delta_0 - \delta_2}\right)^3 - 3\left(\dfrac{\delta - \delta_2}{\delta_0 - \delta_2}\right)^2 + 1 & \delta_2 < \delta < \delta_0 \end{cases}. \tag{4}$$

The two additional shape parameters, δ_1 and δ_2, are used to vary the shape of the traction-separation law. The authors have implemented interface elements as user defined elements into ABAQUS for 2D, shell and 3D models [26, 27]. This implementation also accounts for tangential and mixed mode fracture, but throughout this paper, only mode I fracture is investigated.

The extension of the model presented here contains the triaxiality dependence of the parameters δ_0 and T_0, which is similar to that in [22]. The parameters δ_1 and δ_2 are defined such that the ratios δ_1/δ_0 and δ_2/δ_0, respectively, are kept constant, i.e. the parameters δ_1 and δ_2 vary with h in the same manner as δ_0. Since cohesive elements are not continuum elements, i.e. they don't have a constitutive behaviour of the form $\sigma(\varepsilon)$, the triaxiality cannot be calculated in the cohesive element itself but must be transferred from an adjacent continuum element. For the sake of simplicity, the average of the triaxiality in the nearest element is calculated and transferred afterwards. In addition, no possibility exists in ABAQUS to

calculate and transfer the triaxiality within one increment, but the field quantities can only be transferred to the cohesive model subroutine in the following increment. The error made by this inaccuracy has been evaluated by simulations with different time increments, which did not show a significant deviation (the time increment must be small to achieve convergence anyway).

One important issue for the current investigation is the unloading algorithm. Usually, if only fracture specimens under mode I conditions are considered, local unloading of the cohesive elements, i.e. decreasing separation, does not occur. However, if triaxiality dependence is taken into account, local unloading may occur due to change of the triaxiality, which may lead to an increased cohesive strength. In that case, the status of the cohesive element is an unloading state even if the cohesive stress is kept constant. The algorithm is implemented similar to that in [28], namely the unloading and reloading path is linear and a residual separation remains even after total unloading to the stress free state. This assumption is meaningful for ductile damage, where the voids keep their size after unloading. Negative separations lead to a linear stress path using the initial stiffness. Hence, an overlapping is not prohibited by a penalty parameter, but if the initial stiffness is high enough, the error due to the finite stiffness is negligible. The one-dimensional traction-separation law given in eq. (4) including the unloading/reloading path is shown in Figure 1.

Gelöscht: as well

Gelöscht: Figure 1

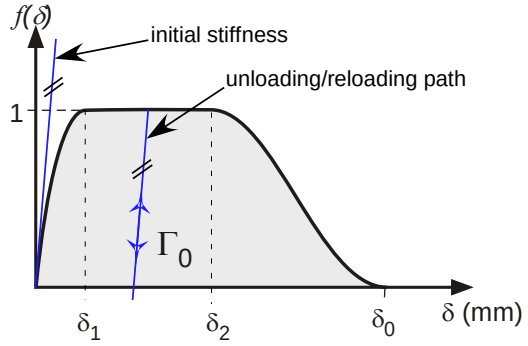

Figure 1: Traction-separation law with two additional shape parameters, δ_1 and δ_2, as given by eq. (4). The stiffness during unloading/reloading is equal to the initial stiffness at zero separation.

Identification of the traction-separation law

A simple 2D axisymmetric single-element test is used for the identification of the traction-separation law. The material under consideration is a ferritic steel used already in [21, 25], which has an initial yield strength of σ_Y = 470 MPa, the initial porosity is f_0 = 0.0025; more detailed values are given in the above reference. However, the simulations performed with the Gurson-model are different in that a single axisymmetric element is calculated here, whereas a plane strain element has been used in [21]. The loading type is equal in both simulations, namely a stress, σ_{appl} is applied in vertical direction, and a constant fraction of the load, β σ_{appl}, ($\beta < 1$) is applied to the horizontal direction. From fraction β, the triaxiality inside the element can then be calculated to

$$h = \frac{2\beta + 1}{3(1-\beta)} \tag{5}$$

Opposite to a simulation with plane strain elements, the triaxiality remains constant until total failure, if an axisymmetric element is used. As a result, the applied stress and the vertical

displacement are evaluated. Of course the total energy dissipated by the Gurson element until total failure depends on the size of the element. Since only energy per cracked area is a meaningful quantity for fracture mechanics, the displacement must be scaled with the "correct" height of the element, D_{cell}, which can be treated as an additional model parameter for the Gurson model. For the material under consideration, the element height should be $D_{cell} = 100$ µm. The cohesive model, on the other hand, reduces the fracture process zone to a plane with zero height, and therefore no such length scale must be taken into account there.

Triaxiality values between 1.0 and 4.0 (resulting in β between 0.4 and 0.786) have been considered, and the cohesion-decohesion curves, $\sigma_{appl}(u_{cell})$, are shown in Figure 2 in accordance to [21]. One can see that the area under the curves, which show the dissipated energy until failure, γ, depend strongly on the triaxiality, as well as the maximum stress, $\sigma_{appl,max}$, especially for low triaxiality. The values of γ and $\sigma_{appl,max}$ are plotted in Figure 2 (right).

Several things are worth noting with respect to these results:

1. The value of $\sigma_{appl,max}$ increases until a triaxiality $h = 2.4$ and then decreases slightly before increasing again. This behaviour is different from the results in [21], where the plane strain element leads to a slight increase until $h = 3.0$ and a constant value thereafter.
2. Due to the Lueders' Plateau of the material, the curves are not smooth, but show a kink at $u_{cell}/D_{cell} \approx 0.025$. This leads to a second local maximum for high triaxialities.
3. Due to the nature of the GTN model, damage may not occur in the elastic regime. However, if plasticity occurs, it cannot be distinguished between plasticity and material separation.

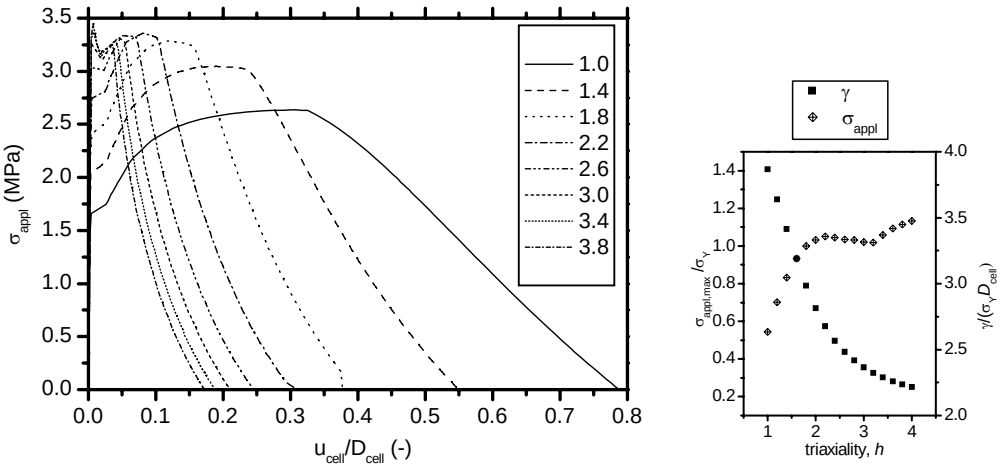

Figure 2: Left: GTN unit cell simulations under various triaxiality values. Right: stress, $\sigma_{appl,max}$, and dissipated energy, γ, of the curves shown on the left as a function of triaxiality, *h*.

The second step is to adjust the parameters T_0 and Γ_0, or T_0 and δ_0, of the cohesive model to meet the curves for $\sigma_{appl,max}$ and γ, respectively, in Figure 2. An additional constraint condition is that in the current implementation the shape parameter δ_2 must have a constant ratio δ_2/δ_0. A least square fit, in which four parameters are varied, yielded best overall results for $\delta_1/\delta_0 = 0.1$ and $\delta_2/\delta_0 = 0.2$.

Gelöscht: Figure 2

Gelöscht: Figure 2

Gelöscht: Figure 2

In order to achieve a good numerical convergence, the symbols in Figure 2 (right) are approximated by a smooth function, similar to the one used in [21][1]. For the present case, the curves follow the equations

$$T_0/\sigma_Y = 3.44 - 4.8\exp\left(\frac{0.1-h}{0.5}\right)$$
$$\delta_0/D_{\text{cell}} = 0.12 + 0.846\exp\left(\frac{0.963-h}{0.797}\right). \quad (6)$$
$$\Gamma_0 = \frac{17}{30}\delta_0 T_0$$

In Figure 3, the approximation of the traction-separation law for two distinct values of h, namely 1.4 and 2.6, are shown. It must be noticed that the general shape of the traction-separation law used in [21] is different from the one used here, which might be another reason for a different fit of the triaxiality dependent parameters.

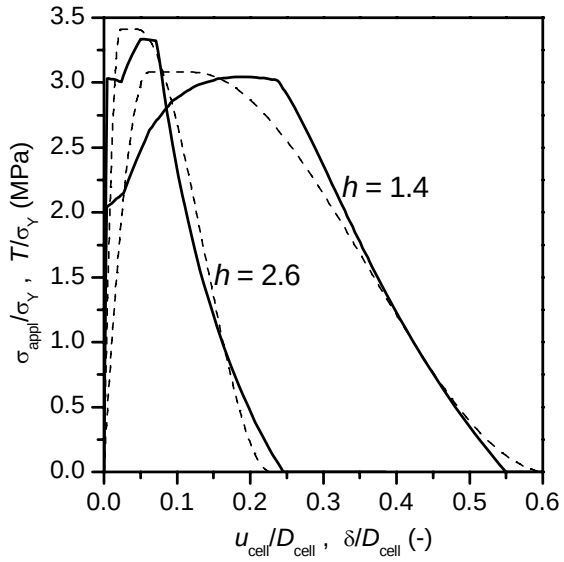

Figure 3: GTN unit cell results (solid lines) and approximation of the traction-separation law based on eq. (4) (dashed lines).

As mentioned initially, the GTN unit cell contains both deformation and damage, whereas the cohesive model is an interface representation of the fracture process zone, which contains material separation only. Since it is not possible to divide the curves of Figure 2 in a deformation part and a damage part, one has to compare the GTN single element with an element of matrix material under J_2 (von Mises) plasticity. The latter contains pure deformation, and therefore the displacement difference between these two curves can be treated as separation, see the solid and the dashed curves in the left graph of Figure 4. When the maximum applied stress has passed, it is assumed that the process contains separation

[1] Eq. (8) in [21] and eq. (7) in [25] contain an error, since the printed functions do not lead to the curves plotted in the corresponding figures.

only. If the elastic displacement in the material is small compared to the plastic displacement, the deformation u_{def} remains constant and the separation can be written as

$$u_{\mathrm{sep}} = \begin{cases} u - u_{\mathrm{def}} & u < u(\sigma_{\max}) \\ u - u_{\mathrm{def}}(\sigma_{\max}) & u > u(\sigma_{\max}) \end{cases} \tag{7}$$

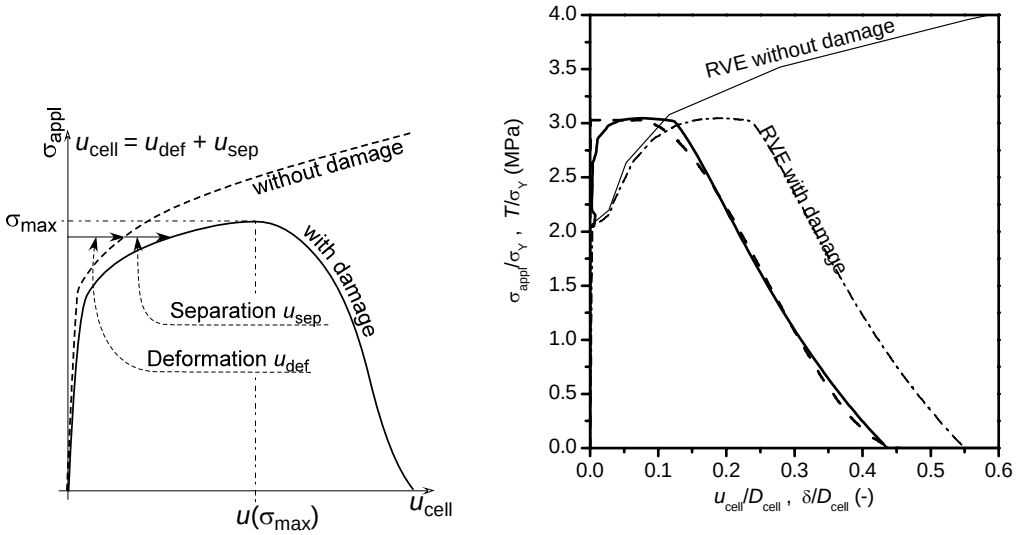

Figure 4: Left: Principal sketch showing the division of the cell displacement into separation and deformation. Right: Generation of a "pure separation" cohesion-decohesion behaviour shown for the triaxiality $h = 1.4$. The dashed line shows the approximation of the traction-separation law based on eq. (4).

After subtracting the deformation from the total cell displacement, the four parameters of the traction-separation law are fitted to the resulting curves. In this case best overall results are achieved with $\delta_1/\delta_0 = 0.001$ and $\delta_2/\delta_0 = 0.15$. The triaxiality dependence of the remaining parameters, T_0 and δ_0, are again approximated by exponential functions:

$$\begin{aligned} T_0/\sigma_Y &= 3.3 - 4.8\exp\left(\frac{0.1-h}{0.45}\right) \quad , \\ \delta_0/D_{\mathrm{cell}} &= 0.138 + 0.635\exp\left(\frac{0.858-h}{0.788}\right) \\ \Gamma_0 &= \frac{23}{40}\delta_0 T_0 \end{aligned} \tag{8}$$

One may notice that the equations for T_0 are different in eqs. (6) and (8), even though the maximum applied stress does not change due to the procedure applied. This is due to least square fit, which does not try to meet the maximum stress but only minimizes the error of the whole curve.

In order to distinguish between the two descriptions of the traction-separation laws, the first one is called *def-sep* model, since it contains the deformation and the separation of the unit cell, whereas the latter is the *pure-sep* model, since it only contains the material separation. The triaxiality dependent parameters of both models are summarised in Figure 5. In the following section they are applied to two different fracture specimens at the structural scale to see whether the new model is able to reproduce both specimens with sufficient accuracy.

Gelöscht: Figure 5

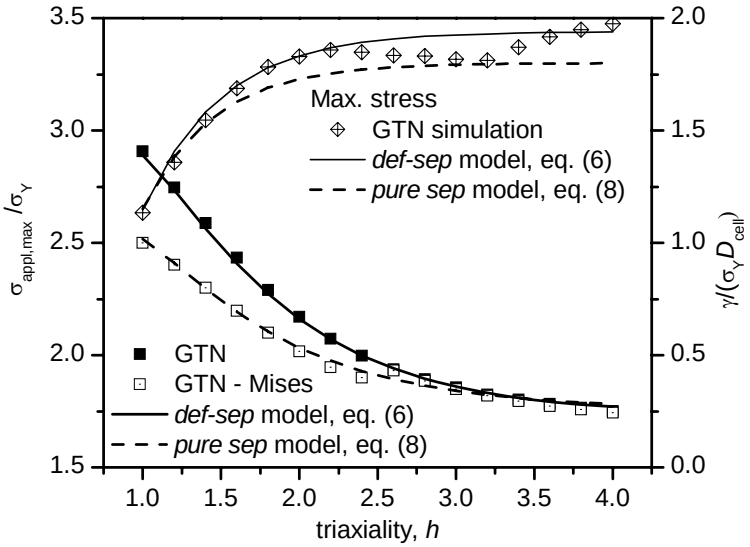

Figure 5: Two different sets of triaxiality dependent parameters for the cohesive model.

Application to fracture mechanics specimens

Standard fracture specimens of side-grooved M(T) and C(T) types have been tested at the German Federal Institute of Materials Testing, BAM, Berlin, see [29]. The geometry of the specimens are: M(T): $W = 50$ mm, $a_0/W = 0.5$, $B = 20$ mm, $B_n = 16$ mm; and C(T): $W = 50$ mm, $a_0/W = 0.59$, $B = 25$ mm, $B_n = 19$ mm. The experimental R curve results in terms of J vs. Δa are reported already in [25]. There, the following simulations have been compared based on the ability to reproduce the results of both experiments:

- GTN model
- Cohesive model with constant parameters (numerically fitted to the experiments)
- Cohesive model with triaxiality dependent parameters (determined from GTN unit cell calculations using the so-called *def-sep* model)

These simulations have been repeated here to receive consistent results. For the GTN simulations the same parameters as in [21] are used; the parameters for the *def-sep* model are those determined in the previous section and the parameters for the triaxiality **in**dependent cohesive model simulations are taken from the approximation of the *pure sep* model at $h = 2$ and not fitted to the experiments. Further simulations are added to this set, i.e. the cohesive model simulations with triaxiality dependent parameters using the so-called *pure sep* model.

Unfortunately, the GTN simulations for the M(T) specimen lead to slightly lower results compared to the those in [25], which might be due to the equation for the J-integral calculation (the current investigation uses the formulae of [30]). However, the tendency is the same, and all simulations have been evaluated using the same procedure, therefore the comparison of the simulations remains valid.

From Figure 6 (left) showing the results for the C(T) specimen, one can see that all simulations give good results regardless the damage model or method of determining the parameters. The results for triaxiality dependent parameters are not very smooth due to strong

Gelöscht: Figure 6

changes in the value of triaxiality at the crack tip, but the tendency is clear, that is both the results for the *pure sep* and the *def-sep* models are very close to the experiment.

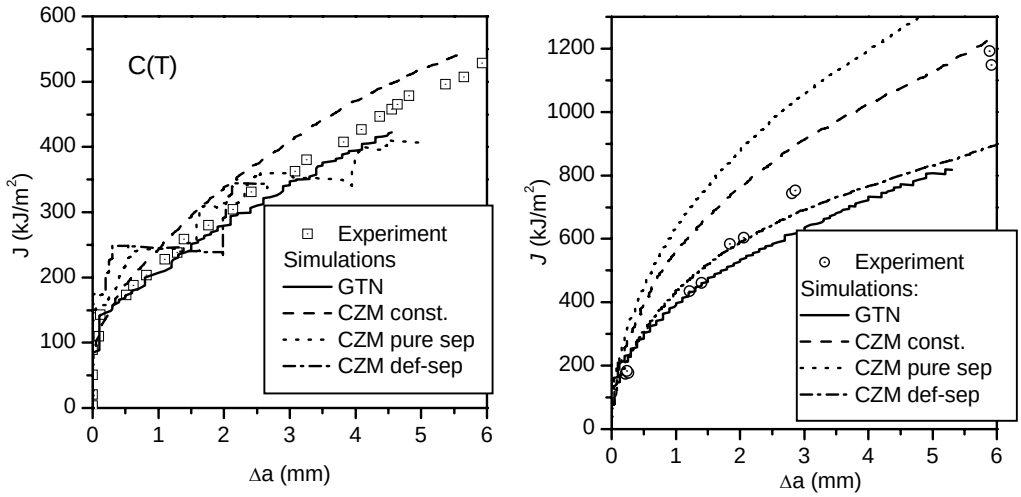

Figure 6: *J* R-curves for C(T) (left) and M(T) specimens (right), experiments and simulations using the GTN model and cohesive model with different parameters.

Larger differences appear for the M(T) specimens. First it is noticed that the experiment does not fit to the GTN simulation very well, which is not reported in [25]. However, the equations used for the experiment are not known in detail and therefore the numerical GTN simulation will be used as reference for the present case.

The most important result is that the cohesive model simulation with triaxiality dependent parameters determined by the *pure sep* model are quite close to the GTN simulation, which was expected. The cohesive model simulations with constant parameters still give reasonable results, but the *J* R-curve determined by the cohesive model simulation using the *def-sep* model is much too steep. The tendency for the simulations performed already in [25] is the same in both works.

Discussion and Conclusions

It must be emphasised that the new method of determining the cohesive parameters in a triaxiality dependent manner, the so-called *pure-sep* model, leads to results that are very similar to those of the GTN model, which they actually should reproduce, even though the elastic unloading has been neglected in the determination of the traction-separation law, and the approximation of the cohesion-decohesion curve by a function as expressed by eq. (4) is rather inaccurate for higher triaxialities.

The results presented in [25] could not exactly be reproduced here, but qualitatively they are similar. The different GTN results in spite of using the same parameters might also be reasoned in a different finite element mesh, since the mesh in the other publication is not known except the requirement of the height of the finite elements along the ligament, which has been set to $D_{cell} = 0.1$ mm. The effect of overestimating the R-curve with the *def-sep* model, on the other hand, is shown again, even more pronounced than in [25], and the results of the cohesive model simulations with constraint independent parameters were closer to the experiment than these, as shown in Figure 6 (right) and also in [25]. Therefore, the idea of

Gelöscht: Figure 6

dividing the cohesion-decohesion curve in a deformation part and a material separation part is justified.

One could argue that the use of the cohesive model is not necessary if the parameters for the GTN model have to be determined beforehand. This is true unless large structures are to be assessed with long crack extension, where GTN simulations tend to run into convergence problems due to loss of stiffness in the continuum elements. However, the main reason for this study is to show that a micromechanical basis for the determination of the cohesive parameters and the shape of the traction-separation law can be found in general. This holds not only for the mechanism of ductile damage, but for any micromechanism that involves material separation. Similar investigations are planned in the future for the description of fibre reinforced composites. In this case the representative volume element, which may contain a number of fibres in different directions, is rather complex, and several damage mechanisms, namely fibre breaking, fibre debonding and matrix damage, are involved. If the damage of such a RVE can be reduced to a single traction-separation law, a significant improvement in the numerical damage simulation of heterogeneous materials will be achieved.

References

1. Gurson, A.L., *Continuum theory of ductile rupture by void nucleation and growth: part I - yield criteria and flow rules for porous ductile media.* J. Eng. Mater. Technol.-Trans. ASME, 1977. **99**: p. 2-15.
2. Tvergaard, V., *On localisation in ductile materials containing spherical voids.* Int. J. Fract., 1982. **18**(4): p. 237-252.
3. Needleman, A. and V. Tvergaard, *An analysis of ductile rupture in notched bars.* J. Mech. Phys. Solids, 1984. **32**(6): p. 461-490.
4. Dugdale, D.S., *Yielding of steel sheets containing slits.* J. Mech. Phys. Solids, 1960. **8**: p. 100-104.
5. Barenblatt, G.I., *The mathematical theory of equilibrium cracks in brittle fracture*. 1962. p. 55-129.
6. Needleman, A., *A continuum model for void nucleation by inclusion debonding.* J. Appl. Mech.-Trans. ASME, 1987. **54**: p. 525-531.
7. Brocks, W., A. Cornec, and I. Scheider, *Computational aspects of nonlinear fracture mechanics*, in *Comprehensive Structural Integrity; Fracture of Materials from Nano to Macro*, I.R. Milne, R.O.\\Karihaloo, B., Editor. 2003, Elsevier. p. 127-209.
8. Tvergaard, V. and J.W. Hutchinson, *The relation between crack growth resistance and fracture process parameters in elastic-plastic solids.* J. Mech. Phys. Solids, 1992. **40**(6): p. 1377-1397.
9. Scheider, I. and W. Brocks, *The effect of the traction separation law on the results of cohesive zone crack propagation analyses.* Key Engineering Materials, 2003. **251-252**: p. 313-318.
10. Volokh, K.Y., *Comparison between cohesive zone models.* Communications in Numerical Methods in Engineering, 2004. **20**(11): p. 845-856.
11. Alfano, G., *On the influence of the shape of the interface law on the application of cohesive-zone models.* Compos. Sci. Technol., 2006. **66**: p. 723-730.
12. Guinea, G.V., M. Elices, and J. Planas, *On the initial shape of the softening function of cohesive materials.* Int. J. Fract., 1997. **87**: p. 139-149.
13. Petersson, P.E., *Crack growth and development of fracture zones in plain concrete and similar materials*. 1981, Lund Institute of Technology.
14. Li, V.C. and R.C. Ward, *A novel testing technique for post-peak tensile behaviour of cementitious materials*, in *Fracture toughness and fracture energy - testing methods*

for concrete and rocks, H. Mihashi, H. Takahashi, and F.H. Wittmann, Editors. 1989, A. A. Balkema Publishers: Rotterdam. p. 183-195.
15. Sorensen, B.F. and T.K. Jacobsen, *Determination of cohesive laws by the J integral approach.* Engineering Fracture Mechanics, 2003. **70**(14): p. 1841-1858.
16. Tvergaard, V., *Model studies of fibre breakage and debonding in a metal reinforced by short fibres.* J. Mech. Phys. Solids, 1993. **41**(8): p. 1309-1326.
17. Steglich, D. and W. Brocks, *Micromechanical modelling of the behaviour of ductile materials including particles.* Comput. Mater. Sci., 1997. **9**: p. 7-17.
18. Peters, P.W.M., J. Hemtenmacher, and W.D. Zeng, in *38. Tagung (Aachen): "Technische Sicherheit, Zuverlässigkeit und Lebensdauer- Bruchmechnik von Grenzflächen"*. 2006, Deutscher Verband für Materialforschung und -prüfung e.V.: Berlin.
19. Broberg, K.B., *The cell model of materials.* Comput. Mech., 1997. **19**: p. 447-452.
20. Siegmund, T. and W. Brocks, *Tensile decohesion by local failure criteria.* Technische Mechanik, 1998. **Band 18**(Heft 4): p. 261-270.
21. Siegmund, T. and W. Brocks, *A numerical study on the correlation between the work of separation and the dissipation rate in ductile fracture.* Eng. Fract. Mech., 2000. **67**: p. 139-154.
22. Anvari, M., I. Scheider, and C. Thaulow, *Simulation of dynamic ductile crack growth using strain-rate and traixiality-dependent cohesive elements.* Eng. Fract. Mech., 2006. **73**: p. 2210-2228.
23. Ivankovic, A., K.C. Pandya, and J.G. Williams, *Crack growth predictions in polyethylene using measured traction-separation curves.* Eng. Fract. Mech., 2004. **71**: p. 657-668.
24. Chen, C.R., et al., *On the determination of the cohesive zone parameters for the modeling of micro-ductile crack growth in thick specimens.* Int. J. Fract., 2003. **120**: p. 517-536.
25. Siegmund, T. and W. Brocks. *The role of cohesive strength and separation energy for modeling of ductile fracture*. in *Fatigue and Fracture Mechanics: 30th Volume*. 2000: ASTM.
26. Scheider, I. and W. Brocks, *Simulation of cup-cone fracture using the cohesive model.* Eng. Fract. Mech., 2003. **70**: p. 1943-1961.
27. Scheider, I. and W. Brocks, *Cohesive elements for thin-walled structures.* Comput. Mater. Sci., 2006. **37**: p. 101-109.
28. Roe, K.L. and T. Siegmund, *An irreversible cohesive zone model for interface fatigue crack growth simulation.* Eng. Fract. Mech., 2003. **70**: p. 209-232.
29. Brocks, W., et al., *Large stable crack growth in fracture mechnics specimens.* Nucl. Eng. Des., 1994. **151**: p. 387-400.
30. *ESIS procedure for determining the fracture behaviour of materials*. 1992, European Structural Integrity Society.